Crosstalk model of a deformable-mirror-based infrared scene projector

Kenneth J. Barnard, MEMBER SPIE
Memphis State University
Department of Electrical Engineering
Memphis, Tennessee 31852
E-mail: barnard@eosms.aa.wpafb.af.mil

Glenn D. Boreman, MEMBER SPIE
University of Central Florida
Center for Research in Electro-Optics and Lasers
Department of Electrical Engineering
Orlando, Florida 32826

Dennis R. Pape, MEMBER SPIE
Photonic Systems Incorporated
1800 Penn Street, Suite 4B
Melbourne, Florida 32901

Abstract. An analytical model for crosstalk is developed for an infrared scene projector that utilizes a deformable-mirror device as an infrared spatial light modulator. Partial-coherence effects that result from the physical layout of the projection system are included. Crosstalk is determined by defining a crosstalk ratio in the projected image. Crosstalk-ratio calculations are carried out for monochromatic and blackbody projection sources over the 3- to 5-μm wavelength band. The results predict crosstalk ratios of 260:1, 1200:1, and 2400:1 for deformable-mirror pixels of 50, 100, and 150 μm when a blackbody source is used in the projection system. Crosstalk performance is improved at shorter wavelengths and for larger deformable-mirror pixels. The results of a proof-of-principle experiment are included to verify the feasibility of a deformable-mirror device in the projection system.

Subject terms: infrared technology; infrared scene projection; deformable mirrors; spatial light modulators; partial coherence.

Optical Engineering 33(1), 140–149 (January 1994).

1 Introduction

The goal of infrared (IR) scene projection is to provide realistic testing and evaluation of infrared-imaging sensors in a controlled laboratory environment. For a valid test, a dynamic spatial and temporal scene that accurately represents real-world targets over a specified wavelength band must be generated. Requirements for scene projection are determined by the sensor under test and can be broken down into several criteria: spatial resolution, dynamic range, contrast ratio, spectral distribution of in-band flux, frame rate, and spatial uniformity.[1–3] The ultimate objective for IR scene projection is hardware-in-the-loop (HWIL) testing of thermal-imaging systems. In HWIL testing, an imaging IR seeker would be mounted on a computer-controlled gimbal and an IR scene generator/projector would present a realistic scene to the seeker, just as would appear in actual use.[4,5] The main difficulty in IR scene projection lies in producing complex scenes of sufficient quality and complexity to characterize today's high-performance IR systems.

The Texas Instruments digital micromirror device[6–10] (TI DMD) has the potential to satisfy current requirements for IR scene projection when used as a spatial light modulator (SLM) for IR radiation from a thermal or laser source. The TI DMD consists of a matrix of discrete reflective elements that can independently tilt in response to an input video signal. A sketch of a portion of the DMD is shown in Fig. 1. Although the DMD can be operated in a bistable mode where the mirror pixels tilt at angles of $+10$ and -10 deg, in this paper, we describe the device as having an off state represented by an untilted pixel and an on state represented by a 10 deg pixel tilt. This particular mode of operation can be achieved by increasing the magnitude of the address voltage of the device.[9] The mirror elements are coated with aluminum as the reflective surface, making the device truly broadband. In addition, the DMD can achieve high frame rates of the order of 10 kHz. In this paper, we present the optical design of an IR scene projector based on the DMD and include the results of a proof-of-principle experiment to verify the validity of the design. A crosstalk model is developed for the system incorporating a DMD with square pixels that tilt along a 45 deg torsion axis. Partial coherence effects are considered in the model.

It is shown that the system behaves coherently under quasi-monochromatic conditions. Also, in the case of blackbody illumination, the spectral characteristics of the source may be approximated as a summation of narrow-band quasimonochromatic sources. Each of these sources produces an independent image-irradiance function in the image plane. The summation of image-irradiance functions gives the total image irradiance, and a crosstalk ratio is determined based on the projected image. Under blackbody illumination, the model predicts crosstalk ratios of 260:1, 1200:1, and 2400:1 for DMD pixel sizes of 50, 100, and 150 μm.

2 Optical Layout

Figure 2 is a layout of the projection system incorporating a blackbody source. Two optical subsystems comprise the complete system: an illumination system and an imaging system. If a laser source is used, the layout is the same except a collimated laser beam replaces the blackbody and collimator. The imaging system is a two-lens relay system that images the DMD plane onto the focal plane of the sensor under test. Relay lens 2 is the lens system of the sensor under test. Together, the two relay lenses produce an overall magnification of $m = -f_2/f_1$, where f_1 and f_2 are the focal lengths of relay lenses 1 and 2. The lens spacing is such that the source is imaged at the entrance pupil of relay lens 2. This

Paper 13013 received Jan. 19, 1993; revised manuscript received May 22, 1993; accepted for publication May 23, 1993.

0091-3286/94/$6.00.

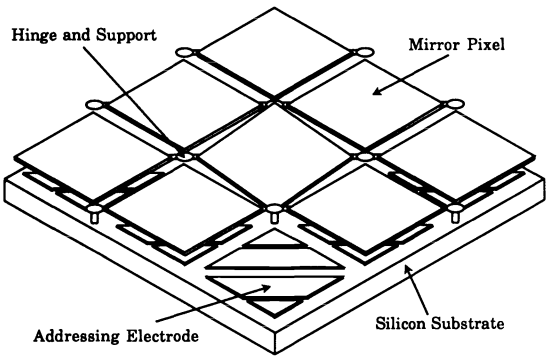

Fig. 1 Sketch of a portion of TI DMD with 45-deg torsion-beam pixels.

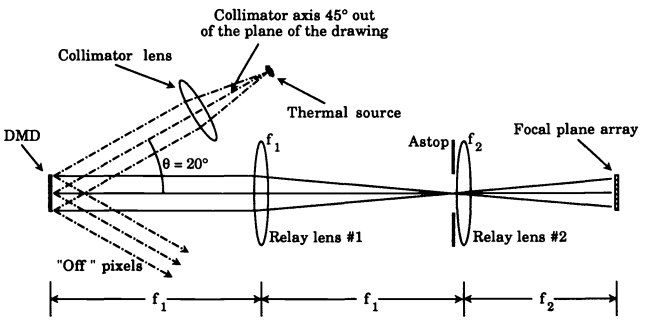

Fig. 2 Optical layout of projection system.

configuration produces a uniform flux distribution across the image plane and minimizes vignetting effects. However, it would be possible to increase the lens spacing and separate the aperture stop from relay lens 2 if necessary. In the case of a coherent source, such as a laser, a Fourier transform plane would exist at the rear focal plane of relay lens 1 and an aperture stop located at this plane would ensure shift-invariant imaging in terms of field amplitude.

Figure 3 is a geometrical model of the projection system operation. The illumination system consists of a thermal source and a collimator. Collimated rays are directed at the DMD at an angle of 20 deg. Rays reflected from the DMD pixels in an untilted off state are directed at an angle of 20 deg from the optical axis. For pixels tilted at an angle of 10 deg, the rays are directed along the optical axis and the pixels are imaged at the sensor focal plane. The arrangement shown is referred to as dark-field illumination because the DMD pixels appear black until tilted to a state that redirects the input radiation along the optical axis of the imaging system. By applying a pulse-width modulation scheme during the integration period of the sensor, gray-level operation can be achieved.

As a verification of operation for the given projector design, a proof-of-principle experiment was performed. The DMD used was a 1000 × 1000 array with 17-μm-square pixels and 45 deg torsion hinges. A filtered tungsten-halogen source with a passband of 0.830 to 1.0 μm was used as the thermal source. A silicon CCD camera was used as a near-infrared imager. For 3- to 5- or 8- to 12-μm operation, a device with larger pixels would be necessary. Figure 4 shows the sensor output for a magnified portion of the DMD array

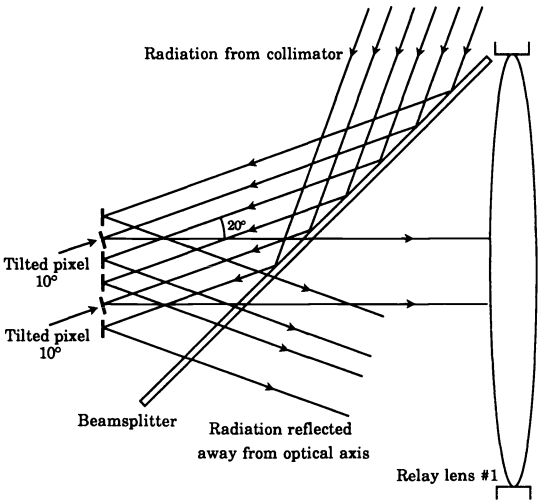

Fig. 3 Geometrical-optics model of DMD operation.

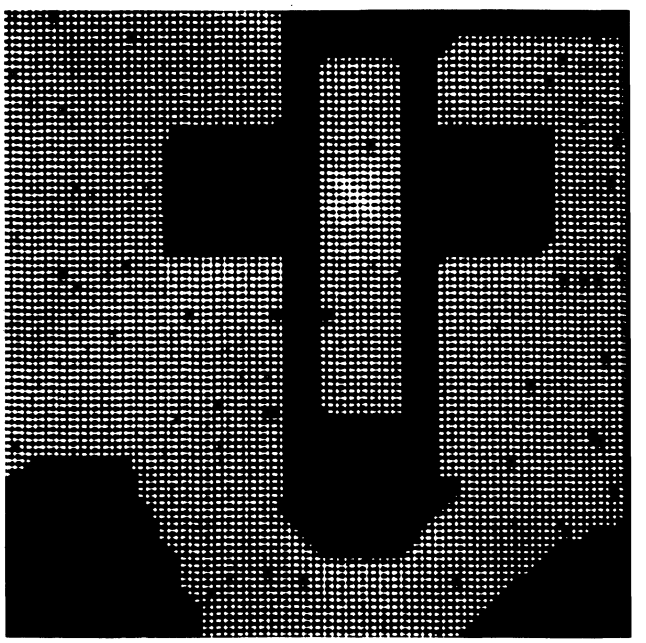

Fig. 4 Near-IR projected scene using a DMD with 17-μm-square pixels and a wavelength passband of 0.830 to 1.0 μm.

for a binary input signal. This figure demonstrates that high-contrast image projection is possible using the DMD as a SLM in an IR scene projector. Note that the DMD used was a demonstration device and did possess pixels that were stuck in either the +10- or −10-deg positions.

3 Partial Coherence Effects

The image-forming process for IR imaging sensors is typically an incoherent process because thermal sources produce essentially incoherent radiation. In many optical systems, such as projection systems with both an illumination system and an imaging system, coherence effects become important.[11] This is the result of the Van Cittert-Zernike theorem, which states that for an extended quasimonochromatic source, spatial coherence improves with decreasing angular

subtense of the source. In a projection system, the source will produce a finite-coherence area at the object plane. If the resolution spot of the imaging system (imaged at the object plane) is smaller than the coherence area of the source at the object plane, the imaging will be approximately coherent. For a resolution-spot size much greater than the coherence area, the imaging will be incoherent. If neither condition is satisfied, the imaging will be partially coherent.

In this section, we determine which imaging regime (coherent, incoherent, or partially coherent) describes the IR scene projector. This analysis is based on a quasimonochromatic source assumption. For the actual projection system, the source is a blackbody and polychromatic source effects are included. Based on these results, we develop an imaging model for the projector.

Starting with a quasimonochromatic source, we determine the mutual-intensity function (MIF) at the object plane. The MIF can then be used to obtain the coherence area. Comparing the coherence area with the diffraction-limited resolution-spot size of the imaging system gives the condition for approximately coherent imaging as

$$z > \frac{3.81 f_1 D_c}{D_i} , \tag{1}$$

where z is the distance between the collimator and the DMD, D_c is the collimator diameter, and D_i is the diameter of the aperture stop located at relay lens 2. Details of the derivation of Eq. (1) are given in Sec. 6. Because of the functional dependencies in Fig. 2, this requirement is independent of the wavelength of the quasimonochromatic source and is a purely geometrical constraint. For the given projector design, D_c and D_i will be on the same order and the distance z must be greater than approximately $4f_1$. This condition can easily be met for typical values of focal lengths and *f/#*s. For our system-design values of $f_1 = 50$ mm, $D_c = 25$ mm, and $D_i = 23$ mm, the requirement for coherent imaging becomes $z > 207$ mm. For values of z less than those of Eq. (1), the imaging system will be partially coherent. By using Eq. (1) as a design constraint, we can force the system to behave coherently. A coherent system ensures linear imaging in terms of field amplitude and enables standard Fourier optics analysis for modeling. For a partially coherent system, imaging characteristics are nonlinear and object dependent.

A one-dimensional partially coherent model of the projector system was developed to verify coherent imaging under the condition given by Eq. (1). To simplify the analysis, the DMD was replaced by a transparent 50-μm slit representing a single DMD pixel. The illumination system was such that the slit was transilluminated along the optical axis. The distance z was chosen to be 300 mm for this analysis and the design values from the previous paragraph were also used. A four-dimensional linear-systems approach incorporating the transmission cross-coefficient was used to characterize the system.[12] The ringing effects in the resultant image-irradiance function shown in Fig. 5 illustrate the coherent effects in the projected image and support the coherent-analysis approach.

The actual source in the projection system is a blackbody, filtered over a spectral band that is much larger than that assumed in the quasimonochromatic analysis. Polychromatic source effects are incorporated to predict actual performance.

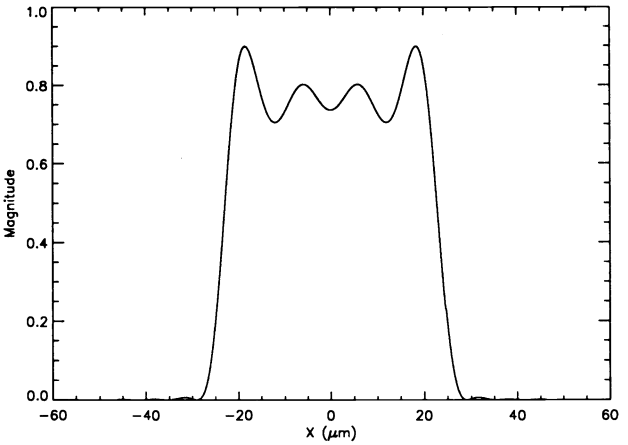

Fig. 5 Image-irradiance function for a 50-μm slit object in the partially coherent model ($\lambda = 3.0$ μm).

In Sec. 6 we derive an approximation of the mutual-coherence function for a polychromatic source based on a summation of narrow-band quasimonochromatic mutual-coherence functions. In imaging applications, each separate mutual-coherence function produces an independent image. The polychromatic image is then given by the summation of the quasimonochromatic image-irradiance functions. The mutual-coherence functions are evaluated at discrete frequencies centered about narrow bands over the passband of interest. Using this approach in conjunction with the quasimonochromatic coherent analysis allows the image irradiance at the focal plane of the sensor under test to be calculated by determining several coherent-image-irradiance functions at discrete wavelengths and then performing a summation over the passband to determine the total image irradiance. The spectral characteristics of the source and the spectral responsivity of the focal plane array must also be included to characterize the performance of the IR projection system.

4 Coherent Model

The ultimate performance limitation of the IR scene projector will be crosstalk in the final image. The crosstalk results from diffraction and will cause off pixels to have some nonzero flux associated with them. An aperture stop in the projection optics eliminates unwanted diffraction orders and its size determines crosstalk performance for a given wavelength. The following analysis provides a theoretical prediction of crosstalk defined in terms of a crosstalk ratio in the final projected image. Standard Fourier optics techniques[13] are used for the case of coherent illumination. Based on the results of the coherent model, polychromatic illumination is assumed for an optimized optical layout and a polychromatic crosstalk ratio is then calculated.

In the coherent model, the imaging system is treated as a linear system in terms of electric-field amplitude and can be written in the spatial frequency domain as

$$U_i(\xi,\eta) = H(\xi,\eta) U_o(\xi,\eta) , \tag{2}$$

where $U_i(\xi,\eta)$ and $U_o(\xi,\eta)$ are the spectrums of the image and object fields, and $H(\xi,\eta)$ is the coherent optical-transfer function. For a coherent system, the optical-transfer function

is simply the scaled exit pupil of the optical system. The object field is given in terms of both the input source field and the reflectance function of the DMD.

We have chosen to define a crosstalk ratio in terms of a specific DMD input where only the center pixel is tilted. This configuration allows us to calculate on-axis crosstalk resulting from a single on pixel. The image-plane crosstalk ratio is found by computing the amount of flux in the geometrical image of the on pixel and the amount of stray flux in the geometrical image of an adjacent off pixel. The crosstalk ratio is defined as the ratio of these two flux values and is given by

$$C=\frac{\int_{\text{on pixel region}} I(x,y)\ \mathrm{d}A_{\text{image}}}{\int_{\text{off pixel region}} I(x,y)\ \mathrm{d}A_{\text{image}}}\ , \tag{3}$$

where C is the defined crosstalk ratio and $I(x,y)$ is the image-irradiance function. This definition of crosstalk ratio is different from the usual low-spatial-frequency definition of contrast ratio in terms of all-dark or all-bright fields. The use of crosstalk ratio yields the pixel-to-pixel crosstalk level that the projector is capable of, for a given set of optical parameters, assuming a particular pixel-array geometry in the sensor under test.

Figure 6 is a cross section of a portion of the DMD with the center pixel tilted at an angle of α and the associated optical fields. The input source field propagates at an angle of 2α and reflects off the DMD. Ignoring constant terms, the source field is a linear-phase plane wave that can be written as

$$u_s(x,y)=\exp\left[jk\frac{\sin(2\alpha)}{\sqrt{2}}(x+y)\right]\ . \tag{4}$$

The reflectance function of the DMD can be written by considering a small portion of the array, as in Fig. 7. For the case of having only the center pixel tilted, the reflectance function can be written as the sum of three terms:

$$r(x,y)=\text{all mirrors off}$$
$$+\text{center mirror on}-\text{center mirror off}\ . \tag{5}$$

The first term in this expression represents the DMD structure

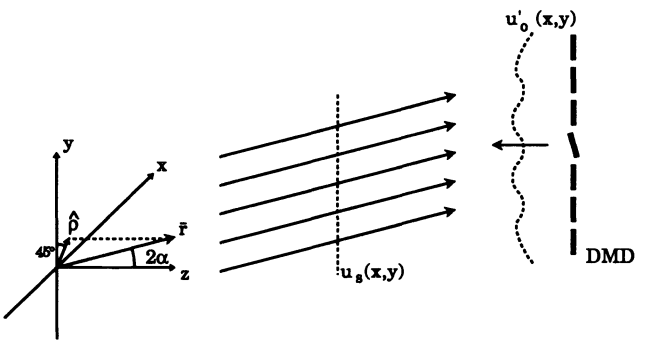

Fig. 6 Input optical fields.

with all mirrors untilted. The second term is a function representing the single tilted center pixel. The last term removes redundancy for the center pixel from the first term. Using standard Fourier optics notation, the reflectance function is given by

$$r(x,y)=\left[\frac{1}{d^2}\ \mathrm{comb}\left(\frac{x}{d},\frac{y}{d}\right)**\ \mathrm{rect}\left(\frac{x}{w'},\frac{y}{w'}\right)\right]\ \mathrm{rect}\left(\frac{x}{D},\frac{y}{D}\right)$$
$$+\exp\left[-jk\frac{\sin(2\alpha)}{\sqrt{2}}(x+y)\right]\ \mathrm{rect}\left(\frac{x}{w},\frac{y}{w}\right)$$
$$-\mathrm{rect}\left(\frac{x}{w'},\frac{y}{w'}\right)\ , \tag{6}$$

where d is the center-to-center pixel spacing, w is the on mirror width, w' is the off mirror width, and D is the total DMD width. The two assumptions made in deriving this expression are that (1) the hinge structure of the pixels is ignored and (2) the tilted pixel shape remains square but reduced in size. A tilted pixel is represented by a skewed rect function and cannot be expressed in a form that is separable in x and y. Substituting a square pixel shape with an area equal to the projected area of the tilted pixel allows the object field to be written in a separable form and simplifies calculation of the image field. The area of the square pixel shape is

$$w^2=w'^2\ \cos(\alpha)\ , \tag{7}$$

where w'^2 is the area of the untilted DMD pixel.

The object-field amplitude is related to the source field and the reflectance function by

$$u'_o(x,y)=u_s(x,y)r(x,y)\ . \tag{8}$$

Substituting Eqs. (4) and (6) into Eq. (8) gives the object field as

$$u'_o(x,y)=\left[\frac{1}{d^2}\ \mathrm{comb}\left(\frac{x}{d},\frac{y}{d}\right)**\ \mathrm{rect}\left(\frac{x}{w'},\frac{y}{w'}\right)\right]$$
$$\times\exp\left[jk\frac{\sin(2\alpha)}{\sqrt{2}}(x+y)\right]\mathrm{rect}\left(\frac{x}{D},\frac{y}{D}\right)+\mathrm{rect}\left(\frac{x}{w},\frac{y}{w}\right)$$
$$-\exp\left[jk\frac{\sin(2\alpha)}{\sqrt{2}}(x+y)\right]\mathrm{rect}\left(\frac{x}{w'},\frac{y}{w'}\right)\ . \tag{9}$$

The object field, scaled to reflect the overall magnification of the optical system, is given by

$$u_o(x,y)=\frac{1}{m}u'_o\left(\frac{x}{m},\frac{y}{m}\right)\ , \tag{10}$$

where $m=-f_2/f_1$ for the two-lens relay system. Substituting Eq. (9) into Eq. (10) and Fourier transforming yields the object field spectrum

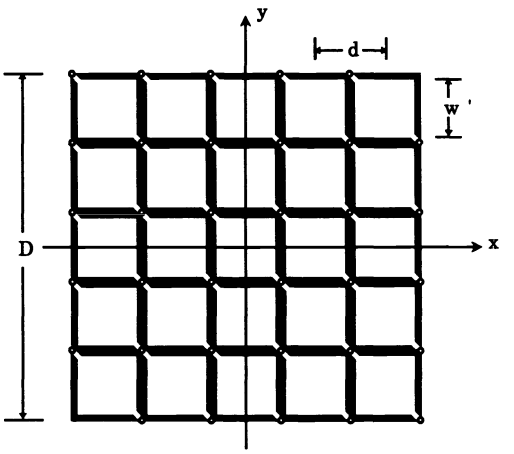

Fig. 7 DMD array geometry for analysis.

$$U_o(\xi,\eta)=m^3w'^2[\mathrm{comb}(md\xi,md\eta)\ \mathrm{sinc}(mw'\xi,mw'\eta)]$$

$$**D^2\ \mathrm{sinc}\left\{mD\left[\xi-\frac{\sin(2\alpha)}{m\lambda\sqrt{2}}\right],\ mD\left[\eta-\frac{\sin(2\alpha)}{m\lambda\sqrt{2}}\right]\right\}$$

$$+mw^2\ \mathrm{sinc}(mw\xi,mw\eta)-mw'^2$$

$$\times\mathrm{sinc}\left\{mw'\left[\xi-\frac{\sin(2\alpha)}{m\lambda\sqrt{2}}\right],\ mw'\left[\eta-\frac{\sin(2\alpha)}{m\lambda\sqrt{2}}\right]\right\}. \quad (11)$$

Equation (11) consists of three terms corresponding to the terms in Eq. (5). The first term produces the overall diffraction pattern of the DMD. It consists of a two-dimensional array of diffraction orders with the zeroth order located off axis. The magnitude of the diffraction orders are weighted by a two-dimensional sinc function corresponding to an untilted pixel. The second term is an on-axis diffraction pattern that results from the single tilted pixel. The last term is the subtracted diffraction pattern of the single untilted pixel.

The coherent optical-transfer function is given by the exit pupil of the imaging system, scaled by the appropriate parameters, as

$$H(\xi,\eta)=\mathrm{cyl}\left[\frac{\lambda f_2}{D_i}(\xi^2+\eta^2)^{1/2}\right]=\begin{cases}1, & 0\leq(\xi^2+\eta^2)^{1/2}<\dfrac{D_i}{2\lambda f_2}\\ \dfrac{1}{2}, & (\xi^2+\eta^2)^{1/2}=\dfrac{D_i}{2\lambda f_2}\\ 0, & (\xi^2+\eta^2)^{1/2}>\dfrac{D_i}{2\lambda f_2}\end{cases}. \quad (12)$$

Multiplying Eqs. (11) and (12) we obtain the image-field spectrum. A subsequent magnitude-squared inverse transform yields the image-irradiance function. To simplify calculation of the inverse transform, only the x axis slice of the two-dimensional image is calculated. The x axis image slice is then used to determine crosstalk ratio along the x direction. The appropriate Fourier-transform pair for this computation is given by

$$u_i(x,0)\leftrightarrow\int_{-\infty}^{\infty}U_i(\xi,\eta)\ d\eta\ . \quad (13)$$

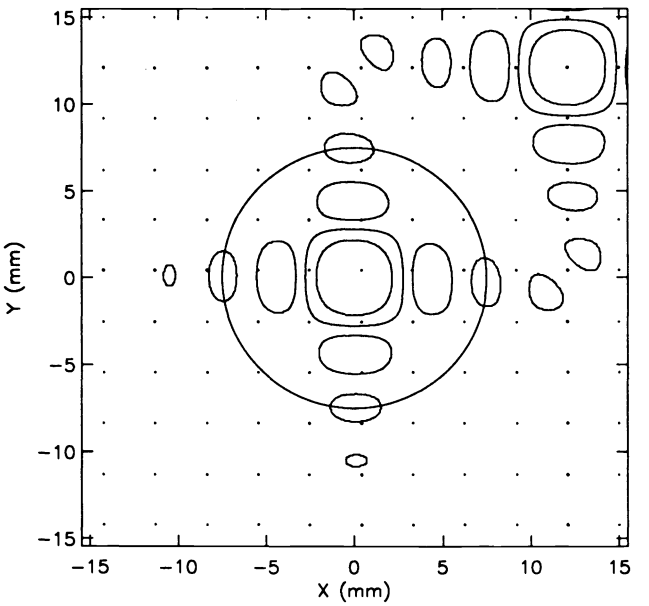

Fig. 8 Contour plot of two-dimensional object-field spectrum and coherent–transfer-function cutoff for a 15-mm-diam aperture stop.

Calculations of crosstalk ratio for an IR scene projector using a 128×128 DMD with pixel sizes of 50, 100, and 150 μm were made. Discrete wavelengths of 3.0, 4.0, and 5.0 μm were used for the coherent analysis. A contour plot of the two-dimensional object field spectrum and cutoff spatial frequency of the coherent transfer function for the case of 50-μm pixels and a wavelength of 3.0 μm is shown in Fig. 8. The axes of the plot are given in terms of aperture stop dimensions so a direct relationship between cutoff frequency and aperture stop size can be made. In this plot, the effects of the three terms that contribute to Eq. (11) can be seen. The diffraction orders produced by the first term are the array of dots in the figure. The zeroth order is located at (12.1 mm, 12.1 mm). It is not evident from this plot, but the orders along $x=12.1$ mm and $y=12.1$ mm have a much larger magnitude than the other diffraction orders shown. The two-dimensional sinc function centered about the origin is the second term in Eq. (11). The subtracted sinc function is shown centered about the zeroth diffraction order. The circular cutoff frequency of the coherent transfer function for a 15-mm aperture stop is overlayed on the plot. The best crosstalk ratio performance will occur when the transfer function passes as much of the spectrum of the single on pixel while blocking out the strong diffraction orders caused by the periodic DMD array.

An upper limit on aperture stop diameter is determined by the location of the large-magnitude diffraction orders in the object spectrum. Using Eqs. (11) and (12), this limit is found from the relation

$$\frac{D_{i\,\max}}{2\lambda f_2}-\frac{\sin(2\alpha)}{m\lambda\sqrt{2}}=0\ . \quad (14)$$

Rewriting Eq. (14) and using $|m|=f_2/f_1$ gives the maximum aperture stop diameter as

$$D_{i\,\max}=f_1\sqrt{2}\ \sin(2\alpha)\ . \quad (15)$$

For an aperture stop diameter less than that given in Eq. (15), the zeroth diffraction order and the other large-magnitude diffraction orders will be blocked.

For the case of a 15-mm aperture, the spectrum of the image-field profile along the x axis was calculated according to Eq. (13) and is shown in Fig. 9. Taking the magnitude squared of the inverse Fourier transform of Fig. 9 gives the image-irradiance function along the x axis in Fig. 10. In this case, the DMD pixel size was 50 μm, and the total flux was calculated over the on pixel width and over an adjacent off pixel width. An area fill factor of 95% was assumed for the DMD pixels. The crosstalk ratio given by the ratio of the two flux values was 170:1 for this particular case. A plot of crosstalk ratio versus aperture stop size is shown in Fig. 11 for wavelengths of 3.0, 4.0, and 5.0 μm. This figure demonstrates that crosstalk ratios greater than 200:1 can be achieved over the wavelength band. Crosstalk ratio plots for DMD pixel sizes of 100 and 150 μm are shown in Figs. 12 and 13. A dramatic improvement in crosstalk ratio is possible as the DMD pixel size increases. From the crosstalk ratio plots, we can see that the crosstalk ratio generally increases until a point where it rapidly falls off. Referring to Eq. (15), this fall off occurs when the transfer function begins to pass the large-magnitude diffraction orders in the object field spectrum. Also present in the crosstalk ratio plots is a periodic trend in the crosstalk ratio as the aperture stop is increased. This is caused by the lobes in the sinc pattern of the on pixel. Depending on where the transfer function cuts through the lobes, the crosstalk performance is improved or degraded.

Based on the analysis in Sec. 7, a blackbody source used in the projection system can be modeled by a coherent approach. The image irradiance is calculated at many discrete wavelengths within the passband of the source and then summed to give the total irradiance. It is necessary that enough wavelengths are used to ensure validity of the quasi-monochromatic conditions over each small wavelength interval. In the polychromatic analysis, we used a blackbody of $T = 1900$ K, with an exitance given by Planck's equation. A linear spectral responsivity given by

$$\mathcal{R}(\lambda) = \frac{\lambda}{\lambda_p}\mathcal{R}(\lambda_p) \ , \tag{16}$$

where $\lambda_p = 5$ μm, was assumed for the detector focal plane array. A wavelength interval of 0.1 μm was chosen and 20 image irradiance samples over the 3- to 5-μm band were

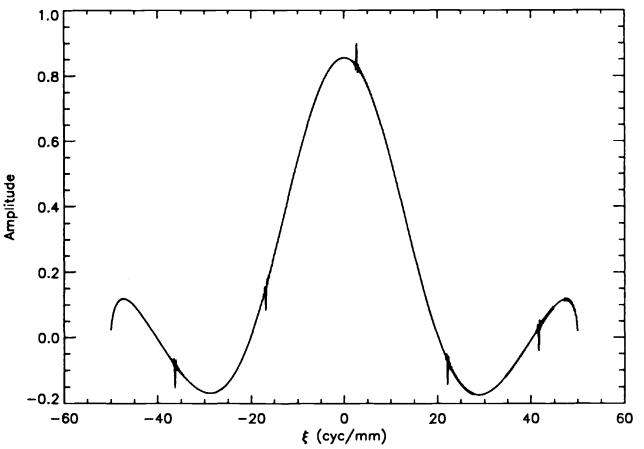

Fig. 9 Spectrum of monochromatic image field along the x axis for a system with a 15-mm-diam aperture stop.

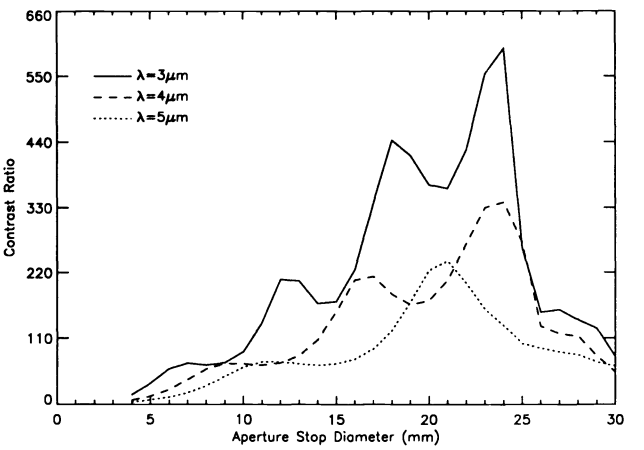

Fig. 11 Crosstalk ratio as a function of aperture stop diameter and wavelength for a 50-μm DMD pixel size.

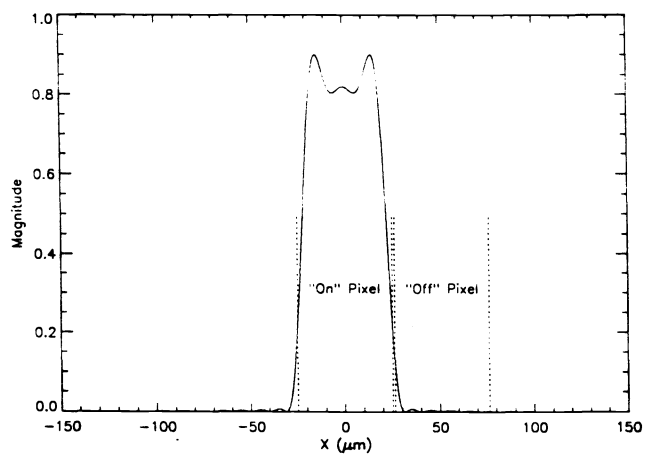

Fig. 10 Monochromatic image irradiance along the x axis for a system with a 15-mm-diam aperture stop.

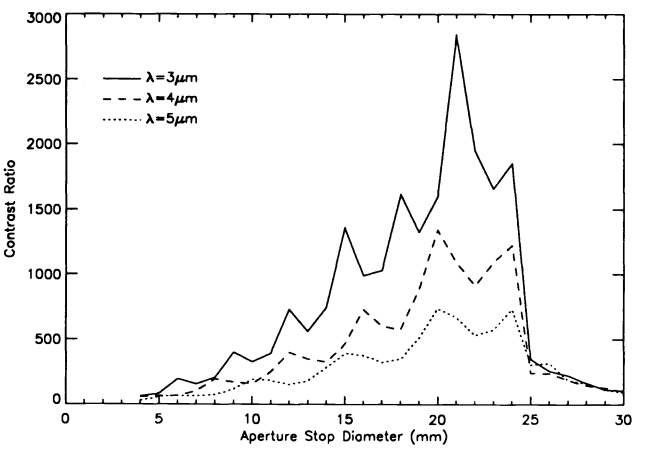

Fig. 12 Crosstalk ratio as a function of aperture stop diameter and wavelength for a 100-μm DMD pixel size.

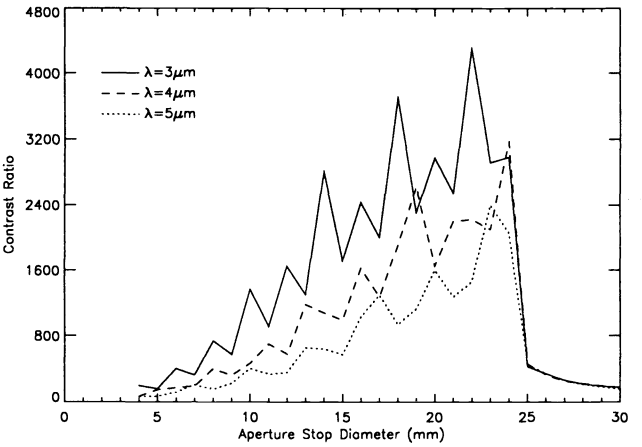

Fig. 13 Crosstalk ratio as a function of aperture stop diameter and wavelength for a 150-μm DMD pixel size.

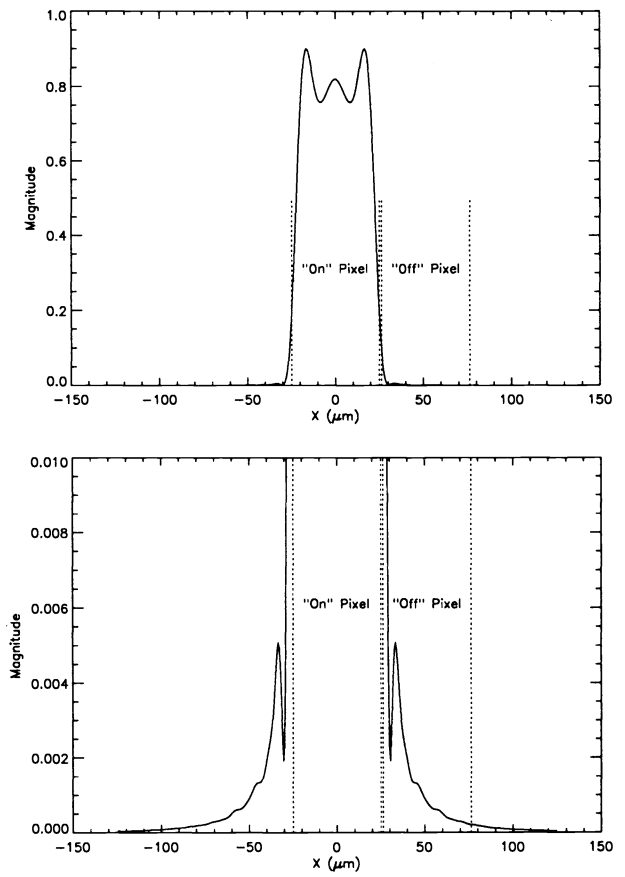

Fig. 14 Total image irradiance along the *x* axis for a 50-μm DMD pixel size and a 23-mm diam aperture stop under polychromatic illumination.

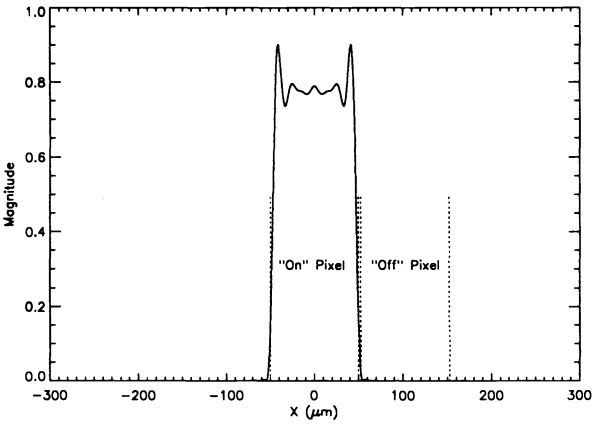

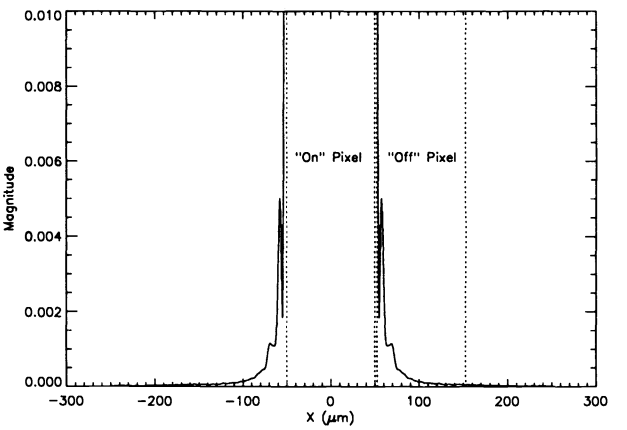

Fig. 15 Total image irradiance along the *x* axis for a 100-μm DMD pixel size and a 23-mm diam aperture stop under polychromatic illumination.

included in the total image-irradiance function. For this case $\nu/\Delta\nu \approx 30$ over the passband. The previous coherent analysis indicates that the best crosstalk performance is obtained when the transfer function just excludes the large-magnitude diffraction orders in the object-field spectrum. Using this criterion, we assumed a fixed aperture stop diameter of 23 mm. The total image-irradiance functions for DMD pixel sizes of 50, 100, and 150 μm are shown in Figs. 14, 15, and 16. The calculated crosstalk ratios for these cases are 260:1, 1200:1, and 2400:1.

5 Conclusions

A DMD-based IR scene projector is capable of high-contrast projection over the 3- to 5-μm band. The feasibility of using a DMD in the projector design was verified in a proof-of-principle experiment. Because of diffraction, the best crosstalk performance occurs at shorter wavelengths and larger DMD pixel sizes. For projection over the 3- to 5-μm band, a DMD pixel size of approximately 100 μm gave a crosstalk ratio in excess of 1000:1.

The particular projector design presented in this paper was based on the assumption that the optical system of the sensor under test is unobscured, as was the optical system in the proof-of-principle experiment. Some IR sensor systems use a Cassegrain objective, which has a central obscuration. A modified projector design that uses a pupil diameter smaller than the central lobe of the DMD diffraction pattern has been investigated[14] for this class of systems.

6 Appendix A: Derivation of Equation (1)

The coherence area of the source illumination at the object plane is found by propagating the MIF from the source to the object plane.[12] The illumination system is shown in Fig. 17 with axes labels at the source, lens, and object planes. In this analysis, the source is assumed to be quasimono-

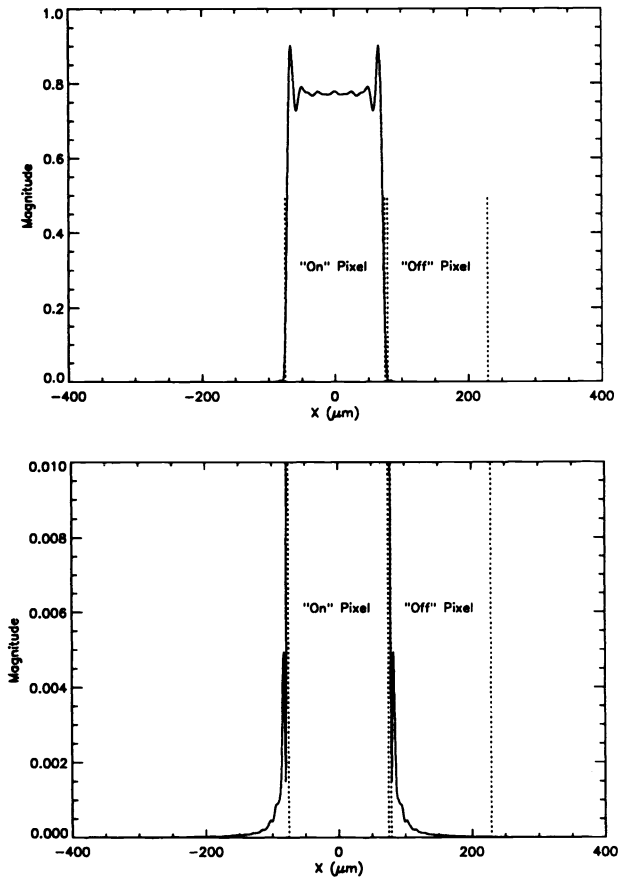

Fig. 16 Total image irradiance along the x axis for a 150-μm DMD pixel size and a 23-mm diam aperture stop under polychromatic illumination.

chromatic and spatially incoherent. Small angles are assumed throughout and a thin-lens approximation is used. Rather than a coherence-area figure of merit, the coherence parameter is given as the maximum separation of two points in the object plane.

Ignoring constant multipliers, the incoherent-source MIF is given by

$$J_s(\alpha_1,\beta_1;\alpha_2,\beta_2)=I_s(\alpha_1,\beta_1)\delta(\alpha_1-\alpha_2,\ \beta_1-\beta_2)\ , \tag{17}$$

where I_s is the source irradiance function; α and β are the source coordinates at points P_1 or P_2, depending on the subscript used; and δ is a Dirac delta function. The s subscript indicates source plane parameters. Using the Van Cittert-Zernike theorem to propagate the source MIF over a distance f gives the MIF at the plane of the collimating lens as

$$J_c(x_1,y_1;x_2,y_2)=\exp\left\{-j\frac{\pi}{\bar{\lambda}f}[(x_2^2+y_2^2)-(x_1^2+y_1^2)]\right\}$$

$$\times\int\int_{-\infty}^{\infty} I_s(\alpha,\beta)\ \exp\left[j\frac{\pi}{\bar{\lambda}f}(\Delta x\alpha+\Delta y\beta)\right]\ d\alpha\ d\beta\ , \tag{18}$$

where $\Delta x=x_2-x_1$ and $\Delta y=y_2-y_1$, and $\bar{\lambda}$ is the mean wavelength of the quasimonochromatic radiation. The c subscript indicates collimator-lens plane parameters. For a lens aperture function $P_c(x,y)$, the MIF transmitted by the lens is given by

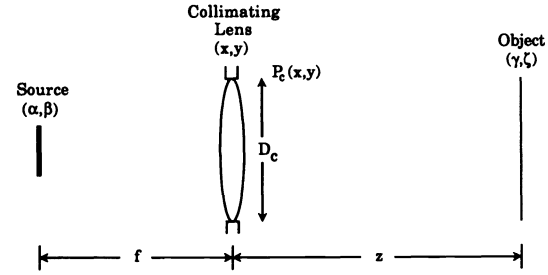

Fig. 17 Illumination system.

$$J_c'(x_1,y_1;x_2,y_2)=P_c(x_1,y_1)P_c^*(x_2,y_2)$$

$$\times\exp\left\{-j\frac{\pi}{\bar{\lambda}f}[(x_1^2+y_1^2)-(x_2^2+y_2^2)]\right\}$$

$$\times J_c(x_1,y_1;x_2,y_2)\ . \tag{19}$$

Substituting Eq. (18) into Eq. (19) and evaluating the Fourier transform integral results in

$$J_c'(x_1,y_1;x_2,y_2)=P_c(x_1,y_1)P_c^*(x_2,y_2)\tilde{I}_s\left(\frac{\Delta x}{\bar{\lambda}f},\frac{\Delta y}{\bar{\lambda}f}\right)\ , \tag{20}$$

where $\tilde{I}_s$ is the two-dimensional spatial Fourier transform of the source irradiance function. The source is assumed to subtend a large enough angle at the lens that the source coherence area at the lens is much smaller than the area of the lens. Under this condition, J_c' will be nonzero only for small values of Δx and Δy, and we can approximate the MIF as

$$J_c'(x_1,y_1;x_2,y_2)\approx|P_c(\bar{x},\bar{y})|^2\tilde{I}_s\left(\frac{\Delta x}{\bar{\lambda}f},\frac{\Delta y}{\bar{\lambda}f}\right)\ , \tag{21}$$

where $\bar{x}=(x_1+x_2)/2$ and $\bar{y}=(y_1+y_2)/2$. Using the Van Cittert-Zernike theorem again to propagate the MIF leaving the lens over a distance z to the object plane gives the object-plane MIF as

$$J_o(\gamma_1,\zeta_1;\gamma_2,\zeta_2)=\exp\left[-j\frac{2\pi}{\bar{\lambda}z}(\bar{\gamma}\Delta\gamma+\bar{\zeta}\Delta\zeta)\right]$$

$$\times\int\int_{-\infty}^{\infty}|P_c(\bar{x},\bar{y})|^2\ \exp\left[j\frac{2\pi}{\bar{\lambda}z}(\bar{x}\Delta\gamma+\bar{y}\Delta\zeta)\right]\ d\bar{x}\ d\bar{y}$$

$$\times\int\int_{-\infty}^{\infty}\tilde{I}_s\left(\frac{\Delta x}{\bar{\lambda}z},\frac{\Delta y}{\bar{\lambda}z}\right)\ \exp\left[j\frac{2\pi}{\bar{\lambda}z}(\bar{\gamma}\Delta x+\bar{\zeta}\Delta y)\right]$$

$$\times d\Delta x\ d\Delta y\ . \tag{22}$$

The o subscript on the MIF indicates that this is an object

plane parameter. In arriving at Eq. (22), the assumption that $\bar{x}\Delta x/z<\bar{\lambda}/4$ and $\bar{y}\Delta y/z<\bar{\lambda}/4$ was made so that an extra phase term could be eliminated. This approximation can be recast as

$$z>2\frac{D_s D_{ca}}{\bar{\lambda}} , \tag{23}$$

where D_s is the maximum dimension of the source and D_{ca} is the maximum dimension of the coherence area of the source at the lens. This requirement can be written in terms of the focal length of the collimating lens as

$$z>\frac{8f}{\pi} , \tag{24}$$

by using relations between the defined coherence area and the area of the source.

Returning to Eq. (22), we see that two Fourier transforms are contained in the expression. The transform of the lens aperture is a narrow function in $(\Delta\gamma,\Delta\zeta)$ compared to the transform that produces a scaled source irradiance function in $(\bar{\gamma},\bar{\zeta})$. This means that the lens aperture determines the coherence area at the object plane and the source determines the average irradiance distribution over the object plane.

The lens aperture function can be written as

$$P_c(x,y)=\mathrm{cyl}\left[\frac{(x^2+y^2)^{1/2}}{D_c}\right]=\begin{cases}1, & 0\leq(x^2+y^2)^{1/2}<\dfrac{D_c}{2}\\ \dfrac{1}{2}, & (x^2+y^2)^{1/2}=\dfrac{D_c}{2}\\ 0, & (x^2+y^2)^{1/2}>\dfrac{D_c}{2}\end{cases} , \tag{25}$$

where D_c is the diameter of the collimating lens aperture. Substituting Eq. (25) into Eq. (22) and ignoring the phase term and the average irradiance term gives the MIF at the object plane as

$$J_o(\gamma_1,\zeta_1;\gamma_2,\zeta_2)\sim 2\frac{J_1[(\pi D_c/\bar{\lambda}z)(\Delta\gamma^2+\Delta\zeta^2)^{1/2}]}{(\pi D_c/\bar{\lambda}z)(\Delta\gamma^2+\Delta\zeta^2)^{1/2}} , \tag{26}$$

where J_1 is the first-order Bessel function of the first kind. If we assume full coherence for $2J_1(r)/r\geq 0.88$, then two points in the object plane with a separation given by

$$s\leq\frac{\bar{\lambda}z}{\pi D_c} , \tag{27}$$

will be coherently illuminated.[15] The radius of the first zero of the diffraction-limited resolution spot of the imaging optics at the object plane is given by

$$\rho=\frac{1.22\bar{\lambda}f_1}{D_i} , \tag{28}$$

where f_1 is the focal length of relay lens 1 of the imaging system and D_i is the diameter of the aperture stop located at relay lens 2. The condition for approximately coherent imaging then becomes

$$z>\frac{3.81 f_1 D_c}{D_i} . \tag{29}$$

This condition is the same as that given in Eq. (1).

7 Appendix B: Quasimonochromatic Approximation of Polychromatic Mutual-Coherence Function

We begin with the expression for the mutual-coherence function of an extended incoherent source, not necessarily quasimonochromatic, derived by Born and Wolf.[15] The source geometry is given in Fig. 18 and shows a small source element dS of the extended source and an observation plane where the mutual coherence between two points P_1 and P_2 is to be calculated. From Section 10.6.1, Eq. (7) of Ref. 15, the mutual-coherence function at the observation plane is given by

$$\Gamma(P_1,P_2,\tau)=\int_0^\infty dv\ \exp(-j2\pi v\tau)\times\int_\sigma I(S,v)\frac{\exp[jk(R_1-R_2)]}{R_1R_2}\,dS , \tag{30}$$

where $I(S,v)$ is the spectral exitance of the source and R_1 and R_2 are the distances from the source point dS and points P_1 and P_2. The spectral characteristics of the source are approximated as a sum of narrow rect functions over the appropriate passband as

$$I(S,v)\approx\sum_n I(S,\bar{v}_n)\frac{1}{\Delta v}\,\mathrm{rect}\left(\frac{v-\bar{v}_n}{\Delta v}\right) , \tag{31}$$

where Δv is the bandwidth and $\bar{v}_n$ is the center frequency of the spectral bands. Substituting Eq. (31) into Eq. (30) and rewriting the wave number k in terms of temporal frequency gives

$$\Gamma(P_1,P_2,\tau)\approx\sum_n\int_0^\infty\frac{1}{\Delta v}\,\mathrm{rect}\left(\frac{v-\bar{v}_n}{\Delta v}\right)\times\exp\left[j2\pi\frac{(v-\bar{v}_n)}{c}(R_1-R_2)\right]\exp(-j2\pi v\tau)\,dv\times\int_\sigma I(S,\bar{v}_n)\frac{\exp[j2\pi(\bar{v}_n/c)(R_1-R_2)]}{R_1R_2}\,dS . \tag{32}$$

Using the quasimonochromatic assumption that $\bar{v}_n\gg\Delta v$ and $|R_1-R_2|\ll c/\Delta v$ for each of the narrow rect spectral bands,

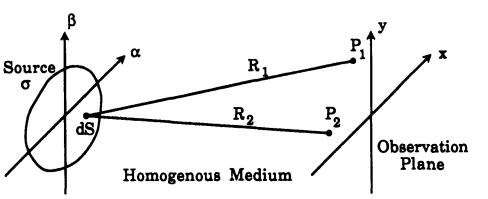

Fig. 18 Extended source and observation plane.

the exponential term $\exp\{-j2\pi[(\nu-\bar{\nu}_n)/c](R_1-R_2)\}$ in the first integral can be approximated as unity. Evaluating the resulting Fourier transform integral and using the Van Cittert-Zernike theorem to replace the integral over the source area by the MIF gives

$$\Gamma(P_1,P_2,\tau)\approx\sum_n \operatorname{sinc}(\Delta\nu\tau)\,J(P_1,P_2,\bar{\nu}_n)\,\exp(-j2\pi\bar{\nu}_n\tau)\ , \tag{33}$$

where $J(P_1,P_2,\bar{\nu}_n)$ is the quasimonochromatic MIF at a frequency of $\bar{\nu}_n$. Because the quasimonochromatic assumption also includes $\Delta\nu|\tau|\ll 1$, Eq. (33) can be further simplified to

$$\Gamma(P_1,P_2,\tau)\approx\sum_n J(P_1,P_2,\bar{\nu}_n)\,\exp(-j2\pi\bar{\nu}_n\tau)\ . \tag{34}$$

In general, the mutual-coherence function under the quasimonochromatic assumption is given as[12]

$$\Gamma(P_1,P_2,\tau)\approx J(P_1,P_2)\,\exp(-j2\pi\bar{\nu}\tau)\ , \tag{35}$$

where $\bar{\nu}$ is the mean frequency of the radiation and $J(P_1, P_2)$ is the MIF. Comparing Eqs. (34) and (35), the polychromatic mutual-coherence function can be written as a summation of independent quasimonochromatic mutual-coherence functions over some passband. In partially coherent imaging applications the time dependence τ, appearing in Eq. (35), is zero and the MIF is propagated through the system to calculate image properties. For polychromatic imaging, each of the independent MIFs in Eq. (34) produces a separate image-irradiance function. The total irradiance function is then given as a summation of individual irradiance functions as

$$I_T(P)\approx\sum_n I(P,\bar{\nu}_n)=\sum_n J(P_1,P_2,\bar{\nu}_n)\big|_{P_1=P_2=P}\ , \tag{36}$$

where I is the quasimonochromatic image irradiance, I_T is the total irradiance, and P represents the coordinates of the image plane.

Acknowledgments

This work was supported by Photonic Systems, Incorporated, Melbourne, Florida, through a Small Business Innovative Research (SBIR) subcontract from the Naval Weapons Center, China Lake, California (Paul Amundson, Contracting Officer's Technical Representative), and by the Florida High Technology and Industry Council. The authors wish to thank Texas Instruments and in particular Jim Florence, for the opportunity to use their facilities and DMD in Dallas, Texas to construct the proof-of-principle projector described in this paper.

References

1. W. E. Woehl, "Transfer requirements for target radiance simulation in optical projection simulators," *Appl. Opt.* **14,** 124–128 (1975).
2. A. P. Pritchard, "Dynamic IR scene generation: basic requirements and comparative display device design," *Proc. SPIE* **940,** 144–149 (1988).
3. T. Barnett, "IR transducer technology: an overview," *Proc. SPIE* **765,** 82–84 (1987).
4. J. L. Hester, "Thermal array target simulation technology," *Proc. SPIE* **940,** 150–152 (1988).
5. D. E. Parker, D. G. Taylor, and C. T. Wallace, Jr., "Trends in scene generation technology: calibration to functional testing," *Proc. SPIE* **1050,** 130–136 (1989).
6. L. J. Hornbeck, "128×128 deformable mirror device," *IEEE Trans. Electron Devices* **ED-30,** 539–545 (1983).
7. D. R. Pape and L. J. Hornbeck, "Characteristics of the deformable mirror device for optical information processing," *Opt. Eng.* **22,** 675–681 (1983).
8. W. R. Wu, R. O. Gale, L. J. Hornbeck, and J. B. Sampsell, "Electro optical performance of an improved deformable mirror device," *Proc. SPIE* **825,** 24–31 (1987).
9. L. J. Hornbeck, "Deformable-mirror spatial light modulators," *Proc. SPIE* **1150,** 86–102 (1989).
10. R. M. Boysel, "Deformable mirror light modulators for image processing," *Proc. SPIE* **1151,** 183–194 (1989).
11. B. J. Thompson, "Image formation with partially coherent light," Chap. IV in *Progress in Optics,* Vol. III, E. Wolf, Ed., pp. 169–230, North Holland Publishing Company, Amsterdam (1969).
12. J. W. Goodman, *Statistical Optics,* pp. 286–324, Wiley, New York (1985).
13. J. D. Gaskill, *Linear Systems, Fourier Transforms, and Optics,* Wiley, New York (1978).
14. J. A. Carter III and D. R. Pape, submitted to *Opt. Eng.*
15. M. Born and E. Wolf, *Principles of Optics,* 6th ed., pp. 511, 532–534, Pergamon Press, New York (1989).

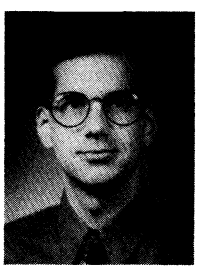

Kenneth J. Barnard received the BS degree in electrical engineering from the University of Michigan in 1986 and MS and PhD degrees in electrical engineering from the University of Central Florida in 1990 and 1992. Dr. Barnard has been at Memphis State University since 1992 and is currently an assistant professor of electrical engineering. His current research interests include infrared scene projection, optical processing, and holography. He is a member of SPIE, OSA, and IEEE.

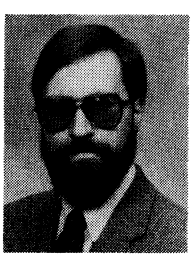

Glenn D. Boreman is an associate professor of electrical engineering in the Center for Research in Electro-Optics and Lasers (CREOL) at the University of Central Florida. He received a BS from the Institute of Optics, University of Rochester, and a PhD from the Optical Sciences Center, University of Arizona. He has held visiting research positions at IT&T, Texas Instruments, U.S. Army Night Vision Lab, and McDonnell Douglas. Dr. Boreman serves as topical editor for *Applied Optics* in the areas of radiometry and detectors and is past-president of the Florida Optical Society.

Dennis R. Pape received a BA degree in physics in 1974 from Cornell University and a PhD in physics in 1980 from Duke University. From 1980 to 1984 he was a member of the technical staff in the Optical Information Processing Branch at Texas Instruments' Central Research Laboratories in Dallas, Texas, where he designed and developed an integrated silicon-based optically addressed membrane spatial light modulator. In 1984 he became the group leader of the Acousto-Optic Device Development Group at Harris Corporation. At Harris he was responsible for the development and application of advanced acousto-optic devices for military optical signal processing systems. In 1987 he founded Photonic Systems Incorporated (PSI) in Melbourne, Florida, where he is the president. He is the author of two book chapters and over 25 papers in the field of optical information processing. He is chairman of the 1992 SPIE meeting on Advances in Optical Information Processing, a member of the technical program committee for the 1992 IEEE Ultrasonics Symposium, and past president of the Florida Section of the OSA. He is also a member of the APS, the Association of Old Crows, and the Air Force Communications and Electronics Association.